RSC Advances

PAPER

View Article Online
View Journal | View Issue

Cite this: *RSC Adv.*, 2017, **7**, 32757

Tuning the spectral, thermal and fluorescent properties of conjugated polymers *via* random copolymerization of hole transporting monomers†

Sapana Jadoun, Syed Marghoob Ashraf ‡ and Ufana Riaz *

With the aim to design conjugated copolymers of hole generating monomers, the present paper reports for the first time, ultrasonic-assisted synthesis of poly(*o*-phenylenediamine) and polycarbazole using different molar ratios of the two monomers. The copolymerization was established by Fourier transform infrared spectroscopy, nuclear magnetic resonance spectroscopy, ultraviolet-visible spectroscopy and differential theromogravimetric analysis while the morphology was investigated using X-ray diffraction and transmission electron microscopy studies. The copolymer composition was confirmed by nuclear magnetic resonance spectroscopy which matched with the molar feed ratio. Reactivity ratios (r_1 and r_2 values) confirmed random copolymerization. Infrared spectra revealed that $\int ad\bar{v}$ values increased with the increase in the poly(*o*-phenylenediamine) units. Cyclic voltammetry also confirmed copolymerization. Oxidation and reduction potentials corresponding to the redox peaks of *o*-phenylenediamine and carbazole copolymers of different composition were close to each other, but fairly different from those of the pure polymers. Redox current densities of copolymers of different compositions were found to vary with the composition. Ultraviolet-visible spectroscopy studies also revealed a progressive change in the optical properties as the copolymer composition changed from 90–10% polycarbazole. X-ray diffraction studies showed morphology of the copolymers to be an intermediate between PCz and POPD where PCz polymer chains appeared least compact and the poly(*o*-phenylenediamine) chains appeared more close and compact. Fluorescence studies confirmed that as the ratio of poly(*o*-phenylenediamine) in the copolymer increased from 30–90%, quantum yield increased from 0.27–0.37. Thermogravimetric analysis and differential theromogravimetric studies confirmed copolymerization of the monomers and showed two types of copolymer complexions which were consistent with the experimentally determined copolymerization ratio.

Received 25th April 2017
Accepted 21st June 2017

DOI: 10.1039/c7ra04662f

rsc.li/rsc-advances

Introduction

Electronically conjugated polymers have drawn considerable attention due to their vibrant applications in low cost opto-electronic devices.[1–5] These materials hold wide scope in designing light-emitting diodes (LEDs) which produce light *via* the recombination of electrons and holes. To achieve high luminescence efficiency, the electron and hole currents must be balanced, implying similar injection and transport behaviour from the two types of carriers. However, typical organic polymers are not good conductors for the simultaneous production of both electrons and holes. Therefore, hetero-structured devices are designed to facilitate charge injection and transport, *via* the insertion of additional charge transport layers in these polymers.[6,7] Such hetero-structured devices show degraded device performance due to phase separation by recrystallization. Controlling phase separation is perhaps the most attractive approach to simultaneously facilitate charge transfer and charge transport.[8–10] Chemists have found copolymerization technique to be one of the best feasible methods for the modification of various physiochemical and optoelectronic properties of homo-polymers as per end use application.[11,12] Conjugated copolymer systems offer the possibility to optimize and tailor electronic and optical properties such as energy transfer and charge transfer which is not feasible in homopolymers. Improved properties can be attained which are generally intermediate between those of its pristine components.[13,14] Galvin *et al.*[15] incorporated oxadiazole units into derivatives of poly(*p*-phenylenevinylene) (PPV), in the main chains and in the side groups which showed improved LED efficiency. Similarly, Kido *et al.*[16] synthesized alternating copolymers of triarylamine (hole transporting) and oxadiazole (electron transporting)

Materials Research Laboratory, Department of Chemistry, Jamia Millia Islamia, New Delhi-110025, India. E-mail: ufana2002@yahoo.co.in

† Electronic supplementary information (ESI) available. See DOI: 10.1039/c7ra04662f

‡ Now retired.

monomers, and demonstrated the use of this copolymer in both undoped and dye-doped LEDs.

Phenylenediamines are bifunctional monomers that can undergo branching/crosslinking when homopolymerized/copolymerized with other monomers.[17] Copolymers of *o*-phenylenediamine with aniline,[18] 2,3-xylidine,[19] *o*-aminophenol,[20] *o*-anisidine,[21] *o*-methoxyaniline,[22] *o*-toluidine,[23] and 1-amino-9,10-anthraquinone[24] are well documented. Poly(carbazole) (PCz) has been rigorously investigated for its optoelectronic properties which are applicable in hole transporting devices.[25] As an organic material, PCz has many advantages because it is inexpensive and can be modulated without increasing steric hindrance near the backbone. Moreover, nitrogen atom can be easily functionalized with a large variety of substituents.[26,27] This study is performed after reviewing the fact that, inspite of the remarkable performance of these two polymers; their monomers have not been copolymerized till date. To explore the hidden potential of combining hole transporting properties of individual homopolymers into one material, carbazole and *o*-phenylenediamine were chosen as key monomers for copolymerization. The effect of copolymerization on the spectral, thermal and morphological properties was investigated. The preparation of copolymers was done *via* ultrasonication technique. Elemental analysis, cyclic voltammetry, nuclear magnetic resonance (^{1}H-NMR), Fourier transform infrared (FTIR) spectroscopy, ultraviolet-visible spectroscopy (UV-vis), fluorescence spectroscopy, thermogravimetry (TGA) and differential thermogravimetric (DTG) measurements were used to establish nature of copolymerization, optical and electronic properties. To investigate morphological features, transmission electron microscopy (TEM) and X-ray diffraction (XRD) analyses were performed.

Experimental

Materials and methods

Carbazole (Cz) (Sigma Aldrich, USA), *o*-phenylenediamine (Sigma Aldrich, USA), ferric chloride (Merck, India), naphthalene sulphonic acid (NSA) (Sigma Aldrich, USA), *N*-methyl-2-pyrrolidone (NMP) (Merck, India), ethanol (Merck, India), tetrahydrofuran (THF) (Merck, India), hydrochloric acid (1 N HCl) (Merck, India), acetonitrile (Merck, India) were used without further purification.

Ultrasonic synthesis of polycarbazole (PCz) and poly(*o*-phenylenediamine) homopolymers

Monomer carbazole (Cz) (1 g, 5.98×10^{-3} mol) was added to 250 ml Erlenmeyer flask containing naphthalene sulphonic acid (NSA) (0.5 g, 2.4×10^{-3} mol) dispersed in deionized water (100 ml). The solution was stirred at room temperature for few minutes. Ferric chloride (1.1 g, 6.17×10^{-3} mol) dissolved in water (50 ml) was added to the above reaction mixture drop by drop with the help of a burette. The flask was then ultrasonicated for 3 h, at 25 °C. Color of mixture turned green. The same was kept in deep freezer for 24 h. The reaction mixture washed several times with distilled water to confirm the removal of excess of ferric chloride which was tested with potassium ferrocyanide. PCz was then dried in a vacuum oven at 70 °C for 72 h to ensure complete removal of impurities and water. Similar procedure was adopted for the synthesis of poly(*o*-phenylenediamine) (POPD) in which the color of the polymer obtained was dark brown.

Ultrasonic copolymerization of carbazole and *o*-phenylenediamine

Synthesis of copolymers of carbazole (Cz) and *o*-phenylenediamine (OPD) was carried out using 7 different molar ratios of Cz : OPD, that is, 90 : 10, 70 : 30, 60 : 40, 50 : 50, 40 : 60, 30 : 70, 10 : 90, respectively (recipe for synthesis given in ESI, Table S1†). The reaction mixture was added to 250 ml Erlenmeyer flask containing NSA (0.5 g, 2.4×10^{-3} mol) dispersed in deionized water (100 ml). The solution was stirred at room temperature for 20 min. Ferric chloride was added to reaction mixture in the ratio of monomer : oxidant (1 : 1 w/w) drop by drop with the help of burette. The flask was then sonicated for 3 h, at 25–30 °C and was kept in deep freezer for 24 h. After that, the reaction mixture washed several times with distilled water to confirm the removal of excess ferric chloride which was tested with potassium ferrocyanide. The copolymer obtained was then dried in a vacuum oven at 70 °C for 72 h to ensure complete removal of impurities and water.

Characterization

Elemental analysis (CHN) of the copolymers was done using a Perkin-Elmer Series II 2400 CHNS/O Analyzer. The viscosity of the homopolymers and copolymers was determined at room temperature using an Ubbehlode viscometer. Cyclic voltammetry was carried out under N_2 atmosphere in three compartment cell on DY 2311 POTENTIOSTAT (Phadke Instruments, India) between the potential range indicated in each figure at 50 mV s^{-1} in concentrated H_2SO_4 using platinum wire as working electrode, a thin platinum loop wire as counter electrode, and Ag/AgCl as reference electrode. Before each measurement, working electrode was washed and polished using velvet cloth with 1 μ alumina powder. FT-IR spectra homopolymers and copolymers were taken in KBr pellets on FT-IR spectrophotometer model Shimadzu IRA Affinity-1. The integrated absorption coefficient, $\int a d\bar{\nu}$, was determined using the IRA Affinity-1 software through Gaussian Lorentzian curve fittings. UV-visible spectra were taken on UV-visible spectrophotometer model Shimadzu UV-1800 using freshly dehydrated NMP and THF as solvents. The oscillator strength was calculated as per method reported in our earlier studies.[28] X-ray diffraction patterns were recorded on Philips PW 3710 powder diffractometer (Nickel filtered copper Kα radiation). The *d* spacing (*D*) was determined using Braggs relation and crystallite size was calculated according to Scherrer equation.[21,28] Transmission electron micrographs (TEM) were taken on Morgagni 268-D TEM, FEI, USA operated at an accelerated voltage of 120 kV. Fluorescence studies were performed on fluorescence spectrophotometer Fluorolog-3 (Horiba) by preparing solutions

of the polymers and copolymers in NMP and THF. The quantum yield Φ was calculated as per method reported in our earlier studies.[28]

Theoretical background of decomposition kinetics study

The solid state decomposition is kinetically described by the general equation

$$\frac{du}{dt} = k_T(u)\cdot f(u) \quad (1)$$

where $k_T(u)$ is the rate constant and $f(u)$ is a function of reaction model. The above rate constant can be equated with Arrhenius rate constant as

$$k_T(u) = A\cdot\exp^{-\frac{E_a}{RT}} \quad (2)$$

where A is the pre exponential factor and E_a is the activation energy, hence the rate equation can be rewritten as

$$\frac{du}{dt} = A\cdot\exp^{-\frac{E_a}{RT}}\cdot f(u) \quad (3)$$

where t is the time and T is the temperature, since

$$\frac{du}{dt} = \frac{du}{dT}\cdot\frac{dT}{dt} \quad (4)$$

where (dT/dt) is the change in temperature of decomposition/minute or rate of heating, °C min^{-1}, β. Hence rate equation in terms of change in temperature can be written as

$$\frac{du}{dT} = \frac{A}{\beta}\exp^{-\frac{E_a}{RT}}\cdot f(u) \quad (5)$$

The above equation can be resolved into usable form employing different mathematical approaches, subjecting to differential or integral treatment.

Ozawa–Flynn–Wall approach

Ozawa, Flynn and Wall[29,30] developed analytical kinetic equations that are not based on any reaction model and hence are more reliable. They are widely used for determining activation energy at different heating rate and different degree of conversion. Ozawa–Flynn–Wall method, eqn (5), after using Doyle's approximation[31] can be written as

$$g(u) = \frac{A}{\beta}\,0.0084\cdot\exp^{\left(-1.052\frac{E_a}{RT}\right)} \quad (6)$$

Taking logarithm of eqn (6), we can write:

$$\ln\beta = \ln\left(\frac{AE_a}{Rg(u)}\right) - 5.3305 - 1.052\,\frac{E_a}{RT} \quad (7)$$

by plotting $\ln(\beta)$ against $1/T$ at different degree of conversion regression lines can be obtained, the slope of these lines will give E_a, activation energy.

Vyazokovin approach

Using Coats–Redfern approximation for temperature integral, eqn (5), can be written as

$$g(u) = \left(\frac{A/\beta RT^2}{E_a}\right)\exp^{\frac{-E_a}{RT}} \quad (8)$$

taking logarithm of eqn (8), and rearranging,

$$\ln\left(\frac{\beta}{T^2}\right) = \ln\left[\frac{RA}{E_a\cdot g(u)}\right] - \left[\frac{E_a}{RT}\right] \quad (9)$$

Regression lines can be drawn by plotting $\ln[\beta/T^2]$ against $1/T$ at different heating rates and at different extent of conversion. The slope of these lines will give activation energy of decomposition.

Friedman approach

Friedman method is a model free equation and is based on the rate of conversion per unit time or per unit temperature and hence is fairly reliable. Taking logarithm of eqn (5),

$$\ln\left(\frac{du}{dt}\right) = \ln\left[\frac{A}{\beta}\right] - \left[\frac{E_a}{RT}\right] + \ln f(u) \quad (10)$$

or

$$\ln\left(\frac{du}{dt}\right) = \ln\left[\frac{A\cdot f(u)}{\beta}\right] - \left[\frac{E_a}{RT}\right] \quad (11)$$

Thus by plotting $\ln[du/dt]$ or $\ln[\beta du/dT]$ *vs.* $1/T$ straight lines will be obtained at different heating rate, the slope of these lies will give activation energy, E_a.

Thermal decomposition was detected in terms of mass loss by using thermal analyzer model Diamond TG/DTA, Perkin Elmer, USA. The temperature change was controlled from room temperature 25 °C to 600 °C at 3 different heating rates of 5 °C, 10 °C, and 15 °C min^{-1}. The sampling segment was set as 0.5 seconds per point and was carried out at low moderate heating rates to keep possible heat/mass-transfer intrusions at minimum. A high purity nitrogen stream (99.5% nitrogen, 0.5% oxygen content) was continuously passed into the furnace at a flow rate of 60 mL min^{-1} at room temperature and atmospheric pressure.

Results and discussion

Confirmation of copolymerization by CHNS, viscosity, cyclic voltammetry, FTIR and ^{1}H-NMR analyses

The homopolymers and copolymers were successfully synthesized *via* chemical polymerization. It was observed that the solubility of the copolymers depended upon the ratio of the monomers present (solubility data given in ESI, Table S2†). The copolymers containing higher number of POPD units were found to be completely soluble in water and most of the organic solvents, whereas the copolymers containing higher number of polycarbazole units showed poor solubility in common organic solvents but fairly good solubility in THF and NMP. Hence, the confirmation of the nature of copolymerization was carried out by CHN and spectral analyses as discussed in the proceeding section.

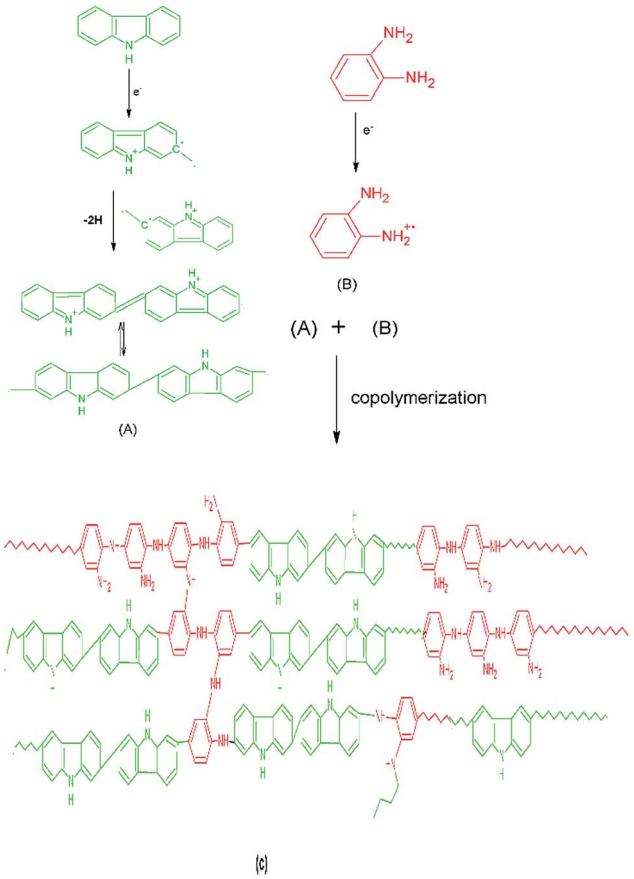

Scheme 1 Copolymerization scheme of PCz with POPD showing the reaction between carbazole dimer (A) with free radicals of *o*-phenylenediamine (B) to form a random copolymer (C).

The scheme of polymerization, Scheme 1, is based on the results obtained from decomposition kinetics which is discussed in later section. Carbazole free radical is highly unstable and shows the tendency to form dimers rapidly which has been well documented in literature.[32,33] Hence, the copolymerization is scheme is shown to proceed *via* the reaction of carbazole dimer with *o*-phenylenediamine, Scheme 1.

It was noticed that the calculated and observed % C in the copolymers differed by a fairly noticeable margin, except copolymer PCz : POPD-90 : 10, % H values differed by 1%, but % *N* values varied between 5–10% (given in ESI Table S3†). Such a noticeable error resulted from some determinational discrepancy. The monomer ratio in the copolymers as determined from CHN varied significantly from the monomer feed ratio particularly in the first and last copolymer samples. This indicated change in the monomer reactivity ratio during the course of polymerization. The reactivity ratios, r_1 and r_2, of these copolymers were calculated, employing Fineman–Ross method[34] based on CHN values.

The ^{1}H-NMR spectra of POPD (given in ESI Fig. S1†) revealed NH proton at $\delta = 6.8$–7.9 ppm, and skeletal NH proton of PCz showed peak from $\delta = 6.9$–8.11 ppm. The overlap of aromatic protons peak of two monomers hinders the assignments of individual peaks in this region to individual monomers. Iraqi *et al.*[35] attributed the peaks at $\delta = 8.15$ ppm (2H) and 7.36 ppm (2H) to 4, 5 and 3, 6 protons of PCz which were also observed in our case and the peak at $\delta = 7.6$ ppm (2H) was related to 1, 8 protons. The above data in our case showed 2–7 linkages in PCz and its copolymer. Intrinsic viscosities of homopolymers were observed to be 0.16 and 0.35 respectively for PCz and POPD. The viscosity average molar mass calculated using Mark-Houwink equation: $[\eta] = KM_v^{\acute{a}}$, where, η is the intrinsic viscosity, $\eta = 1.95 \times 10^{-6} M_v$,[21] M_v is molecular weight; K and $\acute{a}$ are constants for a particular polymer–solvent system. M_v was found to be 4320 for PCz and 6583 for POPD. The intrinsic viscosity of the copolymers varied between the above two limits. These values indicate neither very high nor low molar masses. Li *et al.*[36] have found that when intrinsic viscosity varied between 0.14–0.33, M_n of poly (ethylaniline-*co*-anisidine) varied between 2120–5470 daltons. We have also calculated the molar mass of the copolymers on the basis of the foregoing equation. The monomer reactivity ratios were obtained from the molar feed ratio of PCz and POPD in each copolymer composition, as determined from CHN results, Table 1. Employing the Fineman–Ross (FR) equation,[34] the values of r_1 and r_2, were found as 0.417 and 0.312, (given in ESI Fig. S2†), which revealed random copolymerisation. Table 1 also revealed that in the initial composition containing more carbazole monomer, *i.e.*, PCz : POPD-90 : 10, r_1 appears to be quite high indicating Cz polymerizes in much higher proportion than *o*-phenylenediamine but for the composition around PCz : POPD-10 : 90 containing more *o*-

Table 1 Molar feed ratios determined by ^{1}H-NMR and Fineman Ross parameters

Molar feed ratio of monomer			Molar ratio as determined by ^{1}H-NMR			Fineman Ross parameters	
f_1	f_2	$f = f_1/f_2$	F_1	F_2	$F = F_1/F_2$	$f(F-1)/F$	f^2/F
0.10	0.9	0.11	0.35	0.65	0.54	0.094	0.022
0.3	0.7	0.43	0.40	0.60	0.66	0.22	0.280
0.4	0.6	0.66	0.45	0.55	0.82	0.145	0.532
0.5	0.5	1.0	0.50	0.50	1.0	0.0	1.0
0.6	0.4	1.5	0.55	0.45	1.22	0.27	1.84
0.7	0.3	2.3	0.65	0.35	1.85	1.05	2.859
0.9	0.1	9	0.75	0.25	3.0	6.0	27

Table 2 Oxidation and reduction peaks of homopolymers and copolymers obtained from the cyclic voltammetry studies

Sample	$E_{p\text{-}ox}$ (V)	$I_{p\text{-}ox}$ (μA)	$E_{p\text{-}red}$ (V)	$I_{p\text{-}red}$ (μA)
Pure POPD	0.13(I)	18(I)	−0.05, 0.15(I)	50(I)
Pure PCz	0.3(II)	10(II)	0.5(II)	10(II)
PCz–POPD-10 : 90	0.2(I), 0.35(II)	20(I), 17(II)	−0.025(I), 0.23(II)	4.5(I), 3.5(II)
PCz–POPD: 40 : 60	0.15(I), 0.35(II)	22(I), 11(II)	−0.025(I), 0.23(II)	8(I), 5(II)
PCz : POPD-60 : 40	0.18(I), 0.38(II)	6(I), 3(II)	−0.025(I), 0.35(II)	2(I), 1.5(II)
PCz : POPD: 70 : 30	0.17(I), 0.35(II)	3.6(I), 2.5(II)	−0.02(I), 0.2(II)	2.9(I), 2.5(II)

phenylenediamine monomers, r_2 shows higher extent of polymerisation of *o*-phenylenediamine. In other composition range, polymerisation rate of Cz is little lower than OPD. It has been reported by several authors that carbazole rapidly forms dimers and hence when the molar ratio of carbazole is high, PCz chains are homopolymerized and few POPD units are attached. But when the molar ratio of *o*-phenyenediamine is increased, the extent of homo-polymerization of POPD becomes higher as compared to PCz. However, when the molar ratio is equal, the tendency to copolymerize becomes higher. This observation is also confirmed by the molar ratios determined from ^{1}H-NMR results.

Table 2 shows the redox potential obtained from CV curves (given in ESI Fig. S3†) of PCz, POPD and its copolymers. The $E_{p\text{-}ox}$, potential at the oxidation peak of POPD was noticed to be 0.13 volt and $E_{p\text{-}red}$, potential at the reduction peak of POPD as −0.5 and 0.15 volt, the corresponding current densities, $I_{p\text{-}ox}$, and $I_{p\text{-}red}$ being 18 μA and 50 μA. Likewise the $E_{p\text{-}ox}$, $E_{p\text{-}red}$, $I_{p\text{-}ox}$, and $I_{p\text{-}red}$ values of PCz were respectively found as 0.3 volt, 0.5 volt and 10 μA, 10 μA. Inzlett[37] has shown that the $E_{p\text{-}ox}$ of D^{2+}/D or P^+/P, carbazole dimer and polymer = 0.33 V which matches with our result. Copolymers of POPD and PCz showed an increase in $E_{p\text{-}ox}$ of both the components and a decrease in $E_{p\text{-}red}$ of both the components. Moreover the second reduction potential of POPD, $E_{p\text{-}red}$, 0.15 volt, did not show up in CV of all copolymer composition. $I_{p\text{-}ox}$ POPD and PCz in copolymers where the POPD is more than 50%, is comparable with those of their pure forms. All the above observations clearly confirm the copolymer formation. In the copolymers with POPD(I) being less than 50%, $E_{p\text{-}ox}$, and $E_{p\text{-}red}$, of POPD(I), and PCz(II), behave in the same way, but $I_{p\text{-}ox}$ of components (I) and (II) decrease drastically, while the $I_{p\text{-}red}$ of both the components also decrease. It indicates that oxidation of components (I) and (II) becomes sluggish in the above copolymers.

The FT-IR spectra of homopolymers and copolymers were taken and are given in ESI, Fig. S4.† The band at 3419 cm^{-1} was attributed to –NH– group in PCz, while in POPD, it was observed at 3394 cm^{-1} and in between 3394–3419 cm^{-1} for the copolymers which indicated the presence of secondary amino groups (–NH–) in copolymers. The imine stretching peaks for PCz and POPD were observed to be around 1606 cm^{-1}, 1636 cm^{-1} respectively. The peak of quinonoid units in PCz was noticed at 1512 cm^{-1} while for POPD, it was observed at 1532 cm^{-1} and the absorption intensities of above were found to be 0.13, 0.52 respectively. The peak at 1452 cm^{-1} was attributed to benzenoid form in PCz while in POPD, this peak was observed at 1480 cm^{-1} and absorption intensities of above were found to be 0.36, 0.25 respectively. In this way, the benzenoid to quinonoid ratio (B/Q) was calculated as (0.36/0.13) = 2.76 for PCz, and (0.25/0.52) = 0.48 for POPD demonstrating more benzenoid units in PCz and larger number of quinonoid units POPD. The absorption peak at 1452–1533 cm^{-1} was associated with benzenoid ring stretching vibration which shifted to a higher wave number with increasing *o*-phenylenediamine units. In copolymers, the quinonoid peak possessed higher intensity as compared to that of benzenoid. In copolymers of different ratios (90 : 10, 70 : 30, 60 : 40, 50 : 50, 40 : 60, 30 : 70, 10 : 90) with respect to PCz and POPD, the ratio of absorption intensity of benzenoid to quinonoid was noticed to be 0.750, 0.69, 0.82, 0.8, 0.64, 0.746, 1.02 respectively. Since in the copolymers, the ratio was determined to be below 1.0, the quinonoid units appeared to be slightly higher than benzenoid ones. Both quinonoid and benzenoid forms were present in homopolymer and copolymer chains indicating their conducting nature. The value of $\int ad\bar{v}$ of NH region of PCz (51.10 cm^{-2}) was lower than that of POPD (58.34 cm^{-2}). There was noticeable increase in these values as the loading of POPD increased in the copolymers.

Influence of copolymerization on morphology confirmed by XRD and TEM studies

XRD profile of homopolymer PCz, Fig. 1(a), showed well pronounced peaks at 2θ = 8.5°, 9.2°, 19.7°, 19.9°, 23.4°, 28.2° indicating crystalline structure corresponding to the planes (020), (010), (100), (110) and (011) which were determined on the basis of pseudo orthorhombic lattice.[21] The homopolymer POPD, Fig. 1(b), similarly revealed peaks at 2θ = 9.22°, 18.5°, 19.78°, 23.5° and 28.08°, with only the first peak being pronounced. It also showed crystalline state with limited planes (010), (110) and (011). The copolymers showed peaks of both the homopolymers with slight variation in the positions of some of the peaks along with omission of peaks noticed at 10.76° and 16.66° peaks correlated to POPD. All the peaks are found to be well formed and confirmed crystalline state of the copolymers.[21] It was observed that the copolymers PCz : POPD-90 : 10, PCz : POPD-70 : 30, PCz : POPD-60 : 40, Fig. 1(c)–(e), showed the above peaks, with low intensity, except the peak at 2θ = 9.36° indicating that the number of polymer chains in the corresponding planes were low. But the copolymers PCz : POPD-50 : 50, PCz : POPD-40 : 60, PCz : POPD-30 : 70, PCz : POPD-10 : 90, Fig. 1(f)–(i), with POPD ratio 50% and higher showed

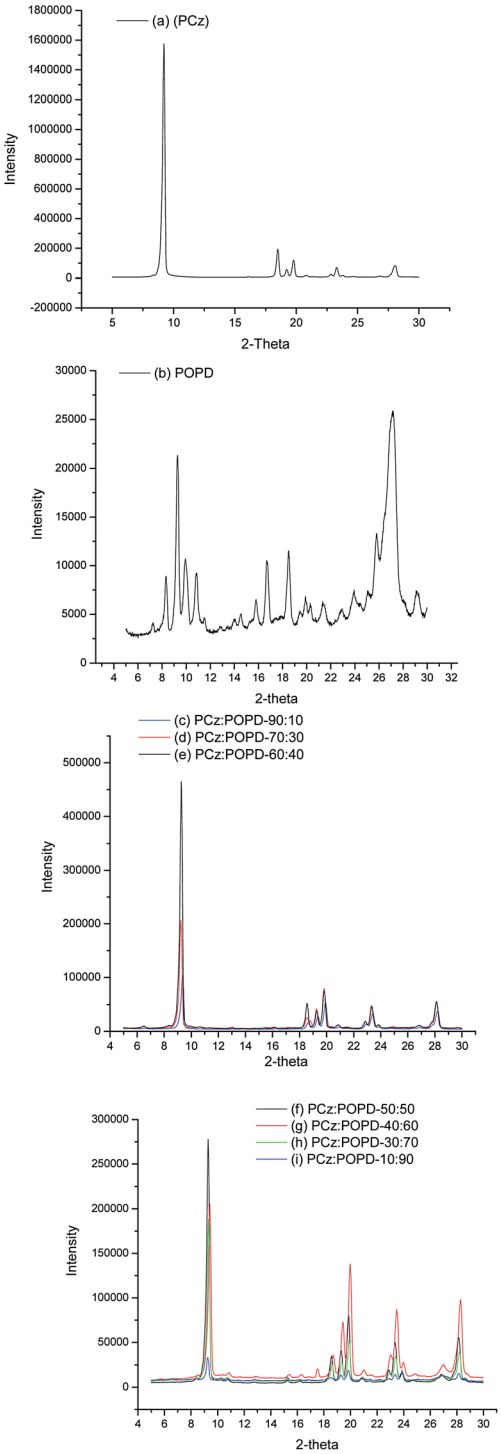

Fig. 1 XRD profiles of (a) PCz, (b) POPD, (c) PCz : POPD-90 : 10, (d) PCz : POPD-70 : 30, (e) PCz : POPD-60 : 40, (f) PCz : POPD-50 : 50, (g) PCz : POPD-40 : 60, (h) PCz : POPD-30 : 70 and (i) PCz : POPD-10 : 90.

high peak intensity which indicated relatively larger number of POPD chains in the corresponding planes.

The TEM of PCz, Fig. 2(a), revealed spherical particles. The particle size was found to be 200 nm. The TEM of POPD, Fig. 2(b), showed fibrillar morphology. The copolymer

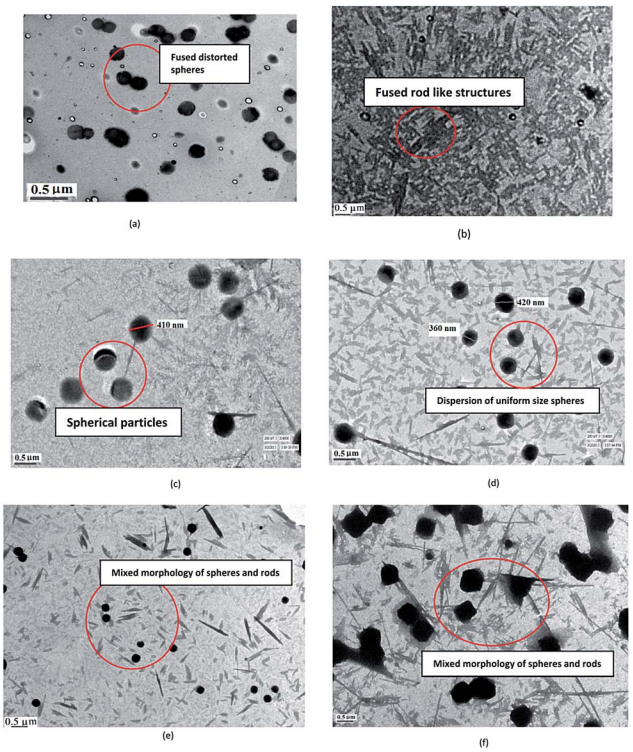

Fig. 2 TEM of (a) PCz, (b) POPD, (c) PCz : POPD-90 : 10, (d) PCz : POPD-70 : 30, (e) PCz : POPD-50 : 50, (f) PCz : POPD-30 : 70.

composition PCz : POPD-90 : 10, Fig. 2(c), revealed predominantly spherical particles matching with the PCz particles. The composition PCz : POPD-70 : 30, Fig. 2(d), showed spherical particles, in case of later, the particles appeared smaller. Some spindle shaped particles were also seen which resembled the morphology found in POPD. The morphology of copolymer PCz : POPD-50 : 50, Fig. 2(e), showed mixed morphology of POPD rod shaped particles along with PCz spheres which were observed to be uniformly scattered. Upon increasing the loading of POPD, PCz : POPD-30 : 70, Fig. 2(f), the PCz particles were observed to be fused together and elongated POPD rods were formed. The morphology of the mixture of POPD and PCz particles (given in ESI Fig. S5†) was found to be quite different from the ones obtained for the copolymers. Dense black aggregates of PCz particles were noticed while POPD particles were found to be randomly dispersed exhibiting highly distorted morphology. The difference in the morphology of the mixture and the copolymers confirmed random copolymerization of PCz with POPD and the copolymers were seen to adopt the morphology of PCz or POPD depending upon the composition.[21]

Influence of copolymerization on the UV-visible and fluorescent properties

The UV-visible spectra of PCz, POPD and its copolymers (taken in NMP) are shown in Fig. 3. Peaks for PCz were observed at 293 nm and 336 nm, while for POPD, they were observed at 280 nm as well as 440 nm. The peaks in the UV range were

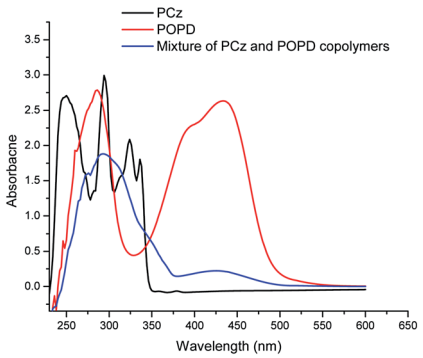

(a)

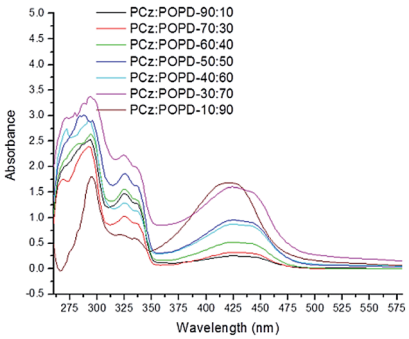

(b)

Fig. 3 UV-visible spectra of (a) PCz, POPD (b) PCz : POPD copolymers.

assigned to π–π* transitions.[21,28] The peak at 425 nm was correlated to polaron formation which indicated the conducting state of the polymer and the transition was associated with the phenazine ring which is conjugated to two lone pairs of electrons on nitrogen atom of the NH_2 groups. The spectra of the mixture of PCz and POPD showed a broad hump at 300 nm and a diffuse hump around 425 nm. Interestingly, the spectra of copolymers were observed to be different from the spectra of the mixture of the two polymers. All the copolymers showed peaks corresponding to both POPD and PCz and their intensities were found to vary with the feed ratio, which confirmed that even during copolymerization, their individual polaronic states were retained. Pure POPD revealed a broad hump spanning from 400–450 nm while in the copolymer, it showed a bathochromic shift of 15 nm. It appeared that some of the electrons on nitrogen were pulled in the phenylene ring. The intensity of the 425 nm peak in copolymer was the lowest for PCz : POPD-90 : 10 (0.2 a.u.) and highest for PCz : POPD-10 : 90 (1.5 a.u.), but the later was much lower than that of pure POPD (2.5 a.u.). This may have been caused by reduction in HOMO–LUMO overlap of the involved orbital in the copolymer. The peak corresponding to POPD in the copolymer varied linearly with the feed ratio. PCz present in the copolymer showed peaks at 290 nm and 325 nm.

Highest intensity peak of 290 nm was noticed for the copolymer in which PCz ratio was second lowest 30 : 70, followed by 50 : 50, 60 : 40, 70 : 30. The peak was correlated to n–π* transition. Because the orientation of pyrrole moiety is upward or downward, transition dipole moment will also adopt the same orientation. At low concentration, the pyrrole moiety in PCz molecules adopts the same orientation, due to the absence of torsional strain and hence their transition dipole moment as well as intensity will be higher. However, when ratio of PCz is higher, the pyrrole moieties in PCz molecules adopt opposite orientation to avoid torsional strain and attain a non-planar configuration. Hence, the dipole moments cancel each other and show lower intensity. As the number of carbazole units increase, the extent of conjugation increases and torsional strain is experienced in a planar conformation. The pyrrole moieties change their orientation to minimize torsional strain and are therefore arranged in a nonplanar conformation. This argument matches with the structure of copolymer depicted in Scheme 1. The molar extinction coefficient and the oscillator strength values for the homopolymers were found to be higher than its copolymers because of the structural variation in the two cases. The molar extinction coefficient and the oscillator strength values of PCz and POPD, respectively decreased and increased as the amount of the two monomers varied in the copolymer, Table 3. Structural changes in the copolymers also contribute to the increase as well as decrease of molar extinction coefficient values. For PCz : POPD-90 : 10, the molar extinction coefficient value ($\acute{\epsilon}_m$) for PCz was found to be 6967.74 while for POPD, it was calculated to be 838.71. For PCz : POPD-70 : 30, $\acute{\epsilon}_m$ value for PCz decreased to 5411.7 and that of POPD increased to 1235.29. Likewise, for copolymer PCz : POPD-50 : 50, $\acute{\epsilon}_m$ value of PCz decreased to 5578.95 with respect to pure PCz while $\acute{\epsilon}_m$ value of POPD increased to 3105.26 with respect to pure POPD. Same trend was found for PCz : POPD 10 : 90, where $\acute{\epsilon}_m$ value for PCz decreased to 3409.09, and for POPD increased to 5909.09. From the copolymer composition, PCz : POPD-90 : 10 up to the copolymer composition, PCz : POPD-60 : 40, the oscillator strength at $\lambda_{max} = 425$ nm for

Table 3 Values of molar extinction coefficient and oscillator strength calculated for PCz, POPD and their copolymers

Sample	λ_{max} (nm)	Molar extinction coefficient	Oscillator strength
PCz	325	8857.14	0.12
POPD	425	9782.61	0.14
PCz : POPD (90 : 10)	325	6967.74	0.10
	425	838.71	0.02
PCz : POPD (70 : 30)	325	5411.76	0.07
	425	1235.29	0.02
PCz : POPD (60 : 40)	325	7111.11	0.04
	425	1722.22	0.03
PCz : POPD (50 : 50)	325	5578.95	0.03
	425	3105.26	0.06
PCz : POPD (40 : 60)	325	4564.10	0.03
	425	2820.51	0.06
PCz : POPD (30 : 70)	325	5951.22	0.02
	425	3707.32	0.08
PCz : POPD (10 : 90)	325	3409.09	0.01
	425	5909.09	0.13

POPD varied between 0.02–0.03 while from the copolymer composition, PCz : POPD-40 : 60 up to the copolymer composition PCz : POPD-10 : 90, it varied between 0.6–0.13. The relatively large increase in oscillator strength for the later compositions indicated structural changes in the copolymer showing the formation of two copolymer complexions.

The fluorescence spectra of PCz, POPD and their various copolymers dissolved in NMP and THF were recorded and are given in Fig. 4. The samples were excited at 400 nm and emission spectra were recorded from 450–700 nm. The emission spectrum of pure PCz and NMP, Fig. 4(a), were also taken which revealed no peak in this region. For the copolymer PCz : POPD-90 : 10 and PCz : POPD-70 : 30 in NMP, a broad peak was noticed at 490 nm which was attributed to $S_1 \rightarrow S_0$ transition. The broadness of the peak was related to intense hydrogen bonding of the two copolymers containing higher PCz content. With the increase in the number of POPD chains, the intensity of this peak appeared to increase and show a shift towards 520 nm. The emission spectra of pure POPD revealed highest intensity peak at 525 nm. The emission spectra for pure THF and pure PCz in THF also revealed the same behaviour. No emission peak of THF was observed upon excitation at 400 nm, Fig. 4(b). With the increase in the POPD content, the emission intensity of the peak corresponding to 525 nm increased progressively. The intensity of the 525 nm peak was observed to increase in both NMP as well as THF with the increase in the

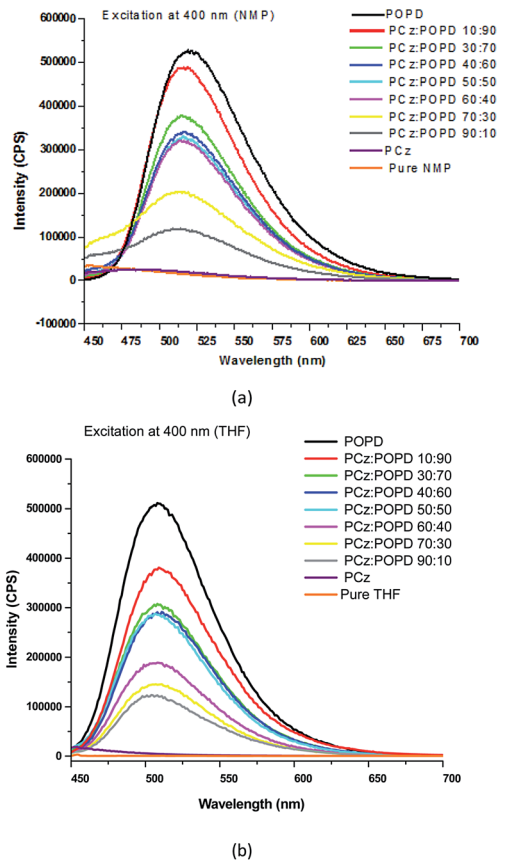

Fig. 4 Fluorescence spectra of PCz, POPD and their copolymers in (a) NMP (b) THF.

Table 4 Quantum yield values for homopolymers and copolymers taken in solution (NMP as solvent)

Sample	λ_{max} (nm)	Integrated area (I_{samp})	Quantum yield (Φ)
PCz	410	3.57×10^8	0.25
POPD	525	1.42×10^9	0.40
PCz : POPD (90 : 10)	500	2.79×10^8	0.24
PCz : POPD (70 : 30)	500	5.03×10^8	0.27
PCz : POPD (60 : 40)	520	8.48×10^8	0.31
PCz : POPD (50 : 50)	520	8.08×10^8	0.30
PCz : POPD (40 : 60)	520	9.51×10^8	0.32
PCz : POPD (30 : 70)	520	8.65×10^8	0.33
PCz : POPD (10 : 90)	520	1.26×10^9	0.37

POPD content. The intensity of the emission peak for the copolymer composition PCz : POPD-10 : 90 was observed to be 510 000 cps in NMP and THF. The copolymer PCz : POPD-30 : 70 revealed an emission intensity of 350 000 cps and 310 000 cps in NMP and THF respectively. But for the composition PCz : POPD-40 : 60 and PCz : POPD-50 : 50, the emission intensities were noticed to be 320 000 cps in NMP and 280 000 and 140 000 cps in THF respectively. The copolymer PCz : POPD-70 : 30 revealed an emission intensity of 210 000

Table 5 Activation energy obtained by F–W–O method, Friedman method and Vyazokovin method

Copolymers PCz : POPD	Degree of conversion (α) (%)	Activation energy (E_a) (kJ mol^{-1}) F–W–O method	Friedman method	Vyazokovin method
90 : 10	10	38.8	28.42	34.93
	20	52.75	43.52	45.76
	30	67.0	59.96	57.90
	40	69.86	65.36	62.2
Average		57.11	49.3	50.21
70 : 30	10	71.42	60.35	65.53
	20	67.55	64.80	68.09
	30	64.75	59.70	62.06
	40	64.95	59.71	61.93
Average		61.67	61.14	64.4
60 : 40	10	71.83	60.35	62.53
	20	71.83	64.89	68.09
	30	66.97	59.71	62.06
	40	66.97	59.71	61.93
Average		69.4	61.16	63.65
40 : 60	10	135.76	132.02	135.27
	20	127.87	124.71	127.12
	30	114.29	110.42	11.28
	40	135.77	132.87	133.39
Average		128.42	125.0	126.7
30 : 70	10	77.17	66.09	69.20
	20	53.43	46.65	47.60
	30	89.34	81.85	84.60
Average		73.85	65.85	67.67
10 : 90	20	280.25	284.92	285.27
	30	99.53	94.33	93.55
	40	41.29	37.08	36.45
Average		140.27	138.77	148.2

cps in NMP and 150 000 in THF respectively. The solvent was therefore found to play little role in the favorable geometrical orientation of HOMO and LUMO orbitals. However the copolymerization was found to push the emission towards near infrared region. Quantum yield (Φ) was calculated by taking Rhodamine B as reference and the values are shown in Table 5 for NMP. The integrated area, $\int ad\bar{v}$, of the peak $\approx$ 525 nm of POPD was calculated to be 1.42×10^9. In the copolymer PCz : POPD-90 : 10, $\int ad\bar{v}$ of the above peak was found to be low, 2.79×10^8. As the ratio of POPD increased in case of PCz : POPD-70 : 30, PCz : POPD-60 : 40, $\int ad\bar{v}$ increased to 5.03×10^8 and 8.48×10^8 respectively. Upon further increasing the POPD ratio to PCz : POPD-40 : 60, PCz : POPD-30 : 70, PCz : POPD-10 : 90, $\int ad\bar{v}$ finally increased to 9.51×10^8 and 8.65×10^8 and 1.26×10^9. Quantum yield of POPD was found to be 0.24 in copolymer PCz : POPD-90 : 10. The quantum yield values were noticed to her higher for the copolymers containing higher POPD content. Similar trend of variation of quantum yield was observed in THF solution (Table 4).

Thermal behavior and decomposition kinetics study of copolymers

TGA-DTG curves for the decomposition of different compositions of PCz:POPD copolymers are given in Fig. 5(a)–(i). Copolymers of composition PCz : POPD-10 : 90 and PCz : POPD-30 : 70, Fig. 5(c) and (d), showed four DTG peaks each. PCz : POPD-10 : 90 showed DTG peaks at 90 °C which was attributed to the evaporation of solvent and water. The second peak at 225 °C was correlated to decomposition of PCz fragments in the copolymer. The peak at 310 °C arose due to the degradation of POPD while the peak at 475 °C was attributed to

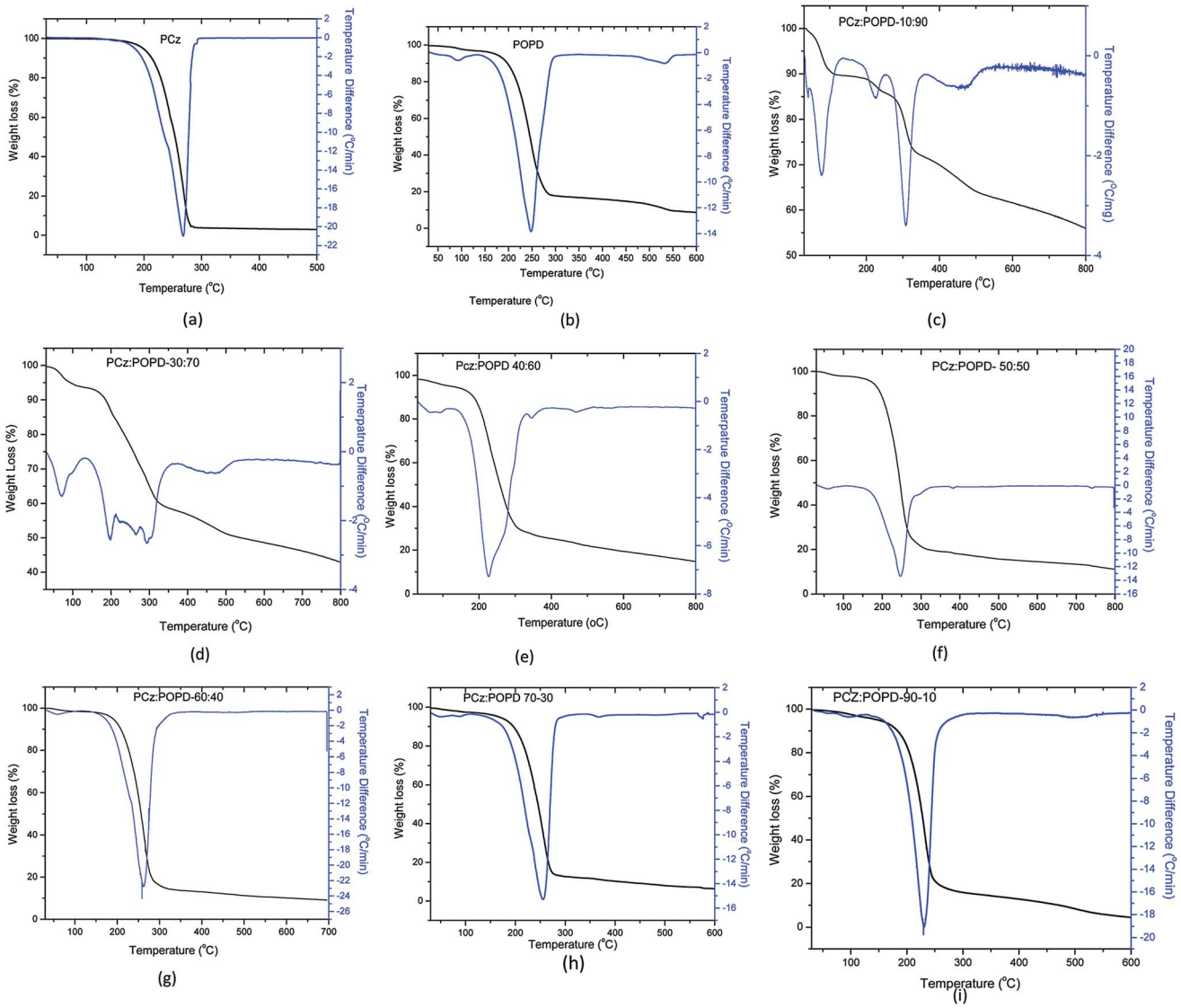

Fig. 5 TGA-DTG plots of (a) PCz, (b) POPD (c) PCz : POPD-10 : 90 (d) PCz : POPD-30 : 70, (e) PCz : POPD-40 : 60, (f) PCz : POPD-50 : 50, (g) PCz : POPD-60 : 40, (h) PCz : POPD-70 : 30, (i) PCz : POPD-90 : 10.

the linkage between PCz and POPD. The char value in this case was found to be 52% which seems to be fairly high. The copolymer PCz : POPD-30 : 70 also showed one solvent evaporation peak along with three decomposition peaks at 60 °C, 200 °C, 300 °C, and 475 °C respectively, like the copolymer PCz : POPD-10 : 90 and the peaks were correlated to decomposition events as in the previous case. The char value was observed to be 45% in this case. A highly pronounced peak of decomposition of PCz at 220 °C and a decomposition peak at 475 °C was associated with POPD, and was also observed in the copolymer PCz : POPD-40 : 60 with a char value of 19%. The copolymers PCz : POPD-60 : 40, PCz : POPD-70 : 30, PCz : POPD-90 : 10, Fig. 5(g)–(i), wherein the PCz content was higher than POPD, showed highly pronounced PCz decomposition peak at 250 °C. The peak due to the decomposition of POPD at 320 °C, solvent evaporation peak at 90 °C, and the PCz–POPD linkage decomposition peak at 475 °C were missing. Incidentally, the char value was calculated to be about 8% in these cases. The decomposition peaks related to POPD and PCz–POPD linkage arose when POPD content in the copolymer was above 60%. This clearly established that PCz complexions in the copolymer were different from each other when POPD content was above and below 60% in the copolymer. When the POPD content was higher than that of PCz, the two polymers formed homopolymers which were weakly linked to each other through hydrogen bonding. Table 5 reveals activation energies at different degrees of conversion determined from Flynn–Wall–Ozawa, Friedman and Vyazokovin methods (plots given in ESI Fig. S6(A–I)†). Activation energies were determined at different degrees of conversion. The values obtained depict that POPD forms linear chains, while PCz forms short oligomers which are grafted on the POPD chains. This explains independent decomposition events of PCz, POPD, and PCz–POPD linkages. The grafting of PCz also stimulates the selective decomposition of POPD into char. When PCz amount was higher than POPD in the copolymer, PCz : POPD-60 : 40, PCz : POPD-70 : 30, and PCz : POPD-90 : 10, only one decomposition event of PCz was observed. It can therefore be concluded that PCz forms main polymer chain tending towards random copolymerization, while POPD is interspersed in the main chain. POPD decomposition event overlaps that of PCz event and the copolymer gives only one decomposition event. The degradation occurred in normal way as pure POPD or pure PCz yielded quite low char value. Low content of POPD in the copolymer reduced the water absorption and caused the disappearance of moisture evaporation peak. Decomposition of polymers is a complex event in which it splits into small free radicals and molecules and even large ones which interact with each other forming amines, aliphatic and aromatic hydrocarbons, phenols and other products.[38,39] Some of these reactions lead to charring. Higher POPD content in the copolymer yielded greater charing because of the presence of larger number of benzene rings in the copolymers. The char value in these copolymers was much higher than in pure POPD which resulted from some synergistic mechanism.[38,39] The above methods therefore justify their use in determining the activation energy of the solid state decomposition of these copolymers. It was observed that the average activation energy of these copolymers determined from each of these methods progressively increased as the amount of POPD in the copolymer increased from 10–90%, except for the composition PCz : POPD-30 : 70, because of certain structural implications as discussed earlier. The average activation energy values of the copolymers PCz : POPD 90 : 10, 70 : 30, 60 : 40, 40 : 60, 30 : 70, 10 : 90 preferentially from Flynn–Wall–Ozawa method was observed to be 57.11, 61.67, 69.4, 128.42, 73.85, and 140.27 kJ mol^{-1}. The other methods gave similar values and exactly same trend. We have already observed that last three copolymers have different monomer complexion than the other three copolymers which is also reflected in their activation energies.

Conclusion

Polycarbazole and poly(*o*-phenylenediamine) were successfully copolymerized *via* ultrasonication technique. Random copolymerization ratio was confirmed by Fineman–Ross equation. Ultraviolet-visible spectroscopy studies revealed the variation in the optical properties as the copolymer composition changed from 90% PCz content (75%-CHN) to 10% PCz content (35%-CHN) which also confirmed random copolymer formation while transmission electron microscopy showed that the copolymers adopted the morphology of polycarbazole/poly(*o*-phenylenediamine) depending upon the composition. Cyclic voltammetry revealed that peak oxidation potential of both polycarbazole and poly(*o*-phenylenediamine) increased in the copolymers while their peak reduction potentials decreased. Thermal analysis revealed random copolymer formation with two different complexions and showed one or more than one decomposition events depending upon copolymer composition. The average activation energy of decomposition of the copolymers containing 90%, 70%, 60%, 40%, 30% and 10% polycarbazole from Flynn–Wall–Ozawa method was observed to be 57.11 kJ mol^{-1}, 61.67 kJ mol^{-1}, 69.4 kJ mol^{-1}, 128.42 kJ mol^{-1}, 73.85 kJ mol^{-1}, and 140.27 kJ mol^{-1}. Fluorescence analysis confirmed that the quantum yield was proportional to the amount of polycarbazole/poly(*o*-phenylenediamine) in the copolymer. The copolymer can be used in designing hetero-structured devices for their application in organic light emitting diodes (OLEDs).

Acknowledgements

The corresponding author DrUfana Riaz wishes to acknowledge the DST-SERB for granting major research project vide sanction number SB/S1/PC-070/2013. One of the co-author Mrs Sapana Jadoun also wishes to acknowledge the DST-SERB for Senior Research fellowship (SRF) under the same project. The authors acknowledge the Sophisticated Analytical Instrumentation Facility at All India Institute of Medical Sciences (AIIMS) for the TEM analysis and the Advance instrumentation Research Facility (AIRF) at JNU, New Delhi, for the fluorescence analysis.

References

1 L. Dou, Y. Liu, Z. Hong, G. Li and Y. Yang, Low-Bandgap Near-IR Conjugated Polymers/Molecules for Organic Electronics, *Chem. Rev.*, 2015, **115**, 12633–12665.

2 U. Riaz, S. M. Ashraf and J. Kashyap, Enhancement of photocatalytic properties of transitional metal oxides using conducting polymers: A mini review, *Mater. Res. Bull.*, 2015, **71**, 75–90.

3 U. Riaz, S. M. Ashraf, R. Raza, K. Kohli and J. Kashyap, Sonochemical Facile Synthesis of Self-Assembled Poly (*o*-phenylenediamine)/Cobalt Ferrite Nanohybrid with Enhanced Photocatalytic Activity, *Ind. Eng. Chem. Res.*, 2016, **55**(22), 6300–6309.

4 U. Riaz, S. M. Ashraf, T. Fatima and S. Jadoun, Tuning the spectral, morphological and photophysical properties of sonochemically synthesized poly (carbazole) using acid Orange, fluorescein and rhodamine 6G, *Spectrochim. Acta, Part A*, 2017, **173**, 986–993.

5 A. Casey, S. D. Dimitrov, P. S. Tuladhar, Z. Fei, M. N. guyen, Y. Han, T. D. Anthopoulos, J. R. Durrant and M. Heenay, Effect of Systematically Tuning Conjugated Donor Polymer Lowest Unoccupied Molecular Orbital Levels *via* Cyano Substitution on Organic Photovoltaic Device Performance, *Chem. Mater.*, 2016, **28**, 5110–5120.

6 K. K. Nanda, S. Swain, B. Satpati, L. Besra, B. Mishra and Y. S. Chaudhary, Enhanced Photocatalytic Activity and Charge Carrier Dynamics of Hetero-Structured Organic–Inorganic Nano-Photocatalysts, *ACS Appl. Mater. Interfaces*, 2015, **7**, 7970–7978.

7 A. Takai, Z. Chen, X. Yu, N. Zhou, T. J. Marks and A. Facchetti, Annulated Thienyl-Vinylene-Thienyl Building Blocks for π-Conjugated Copolymers: Ring Dimensions and Isomeric Structure Effects on π-Conjugation Length and Charge Transport, *Chem. Mater.*, 2016, **28**, 5772–5783.

8 Y. J. Hwang, T. Earmme, B. A. E. Courtright, F. N. Eberle and S. A. Jenekhe, n-Type Semiconducting Naphthalene Diimide-Perylene Diimide Copolymers: Controlling Crystallinity, Blend Morphology, and Compatibility Toward High-Performance All-Polymer Solar Cells, *J. Am. Chem. Soc.*, 2015, **137**, 4424–4434.

9 S. Holliday, R. S. Ashraf, C. B. Nielson, M. Kirkus, J. A. Rohr, C. H. Tan, E. C. Fregoso, A. S. Knall, J. R. Durrant, J. Nelson and I. McCulloch, A Rhodanine Flanked Nonfullerene Acceptor for Solution-Processed Organic Photovoltaics, *J. Am. Chem. Soc.*, 2015, **137**, 898–904.

10 A. Takai, Z. Chen, X. Yu, N. Zhou, T. J. Marks and A. Facchetti, Annulated Thienyl-Vinylene-Thienyl Building Blocks for π-Conjugated Copolymers: Ring Dimensions and Isomeric Structure Effects on π-Conjugation Length and Charge Transport, *Chem. Mater.*, 2016, **28**, 5772–5783.

11 U. Riaz, R. Jahan, S. Ahmad and S. M. Ashraf, Copolymerization of poly (1-naphthylamine) with aniline and *o*-toluidine, *J. Appl. Polym. Sci.*, 2008, **108**(4), 2604–2610.

12 M. Jaymand, M. Hatamzadeh and Y. Omidia, Modification of polythiophene by the incorporation of processable polymeric chains: Recent progress in synthesis and applications, *Prog. Polym. Sci.*, 2015, **47**, 26–69.

13 X. Zhou, N. Ai, Z.-H. Guo, F.-D. Zhuang, Y.-S. Jiang, J.-Y. Wang and J. Pei, Balanced ambipolar organic thin-film transistors operated under ambient conditions: Role of the donor moiety in BDOPV-based conjugated copolymers, *Chem. Mater.*, 2015, **27**, 1815–1820.

14 M. Gao, J. Subbiah, P. B. Geraghty, M. Chen, B. Purushothaman, X. Chen, T. Qin, D. Vak, F. H. Scholes, S. E. Watkins, M. Skidmore, G. J. Wilson, A. B. Holmes, D. J. Jones and W. W. H. Wong, *Chem. Mater.*, 2016, **28**, 3481–3487.

15 Z. Peng, Z. Bao and M. E. Galvin, Oxadiazole-Containing Conjugated Polymers for Light-Emitting Diodes, *Adv. Mater.*, 1998, **10**, 680–684.

16 J. Kido, G. Harada and K. Nagai, Electroluminescent poly (arylene ether) containing both hole-transporting and electron-transporting units, *Chem. Lett.*, 1996, **2**, 161–170.

17 N. M. Adamczyk, A. A. Dameron and S. M. George, Molecular layer deposition of poly (*p*-phenylene terephthalamide) films using terephthaloyl chloride and *p*-phenylenediamine, *Langmuir*, 2008, **24**, 2081–2089.

18 X.-G. Li, H.-Y. Wang and M.-R. Huang, Synthesis, film-forming, and electronic properties of *o*-phenylenediamine copolymers displaying an uncommon tricolor, *Macromolecules*, 2007, **40**, 1489–1496.

19 X.-G. Li, M.-R. Huang and Y. Yang, Synthesis and characterization of *o*-phenylenediamine and xylidine copolymers, *Polymer*, 2001, **42**, 4099–4107.

20 Y. Kong, X. Shan, Y. Tao, Z. Chen and H. Xue, Synthesis of Poly (*o*-phenylenediamine-*co*-*o*-aminophenol) *via* Electrochemical Copolymerization and its Electrical Properties, *J. Electrochem. Soc.*, 2013, **160**, G96–G101.

21 U. Riaz, S. M. Ashraf, S. Aleem, V. Budhiraja and S. Jadoun, Microwave-assisted green synthesis of some nanoconjugated copolymers: characterisation and fluorescence quenching studies with bovine serum albumin, *New J. Chem.*, 2016, **40**, 4643–4653.

22 L. Zhang, W. Yuan and Y. Yan, *In situ* UV–vis spectroelectrochemical studies on the copolymerization of *o*-phenylenediamine and *o*-methoxy aniline, *Electrochim. Acta*, 2013, **113**, 218–228.

23 S. Bilal and R. Holze, Electrochemical copolymerization of *o*-toluidine and *o*-phenylenediamine, *J. Electroanal. Chem.*, 2006, **592**, 1–13.

24 L. A. Hernandez, M. A. Del Vallei, F. J. Armijoi, F. R. Diazi and G. Louarn, Electro-oxidation of 1-amino-9,10-anthraquinone and *O*-phenylenediamine and the Influence of Its Copolymerization in the Modified Electrode Properties, *Electrochemistry*, 2013, **81**, 954–965.

25 U. Riaz, S. M. Ashraf, S. K. Saroj, M. Zeeshan and S. Jadoun, Microwave-assisted solid state intercalation of Rhodamine B and polycarbazole in bentonite clay interlayer space: structural characterization and photophysics of double intercalation, *RSC Adv.*, 2016, **6**(41), 34534–34545.

26 I. B. Ceballos, F. Hermerschmidt, A. V. Akkuratov, D. K. Susarova, P. A. Troshin and S. A. Choulis, High-

Performing Polycarbazole Derivatives for Efficient Solution-Processing of Organic Solar Cells in Air, *ChemSusChem*, 2015, **8**, 4209–4215.

27 H. E. Oğuztürk, S. Tirkes and A. M. Onal, Electrochemical synthesis of new conjugated polymers based on carbazole and furan units, *J. Electroanal. Chem.*, 2015, **750**, 1–8.

28 U. Riaz and S. M. Ashraf, Microwave-assisted solid state *in situ* polymerization and intercalation of poly (carbazole) between bentonite layers: effect of microwave irradiation and gallery, *J. Phys. Chem. C*, 2012, **116**, 12366–12372.

29 T. Ozawa, A new method of analyzing thermogravimetric data, *Bull. Chem. Soc. Jpn.*, 1965, **38**, 1881–1886.

30 J. H. Flynn, The 'temperature integral'—its use and abuse, *Thermochim. Acta*, 1997, **300**, 83–92.

31 C. D. Doyle, Kinetic Analysis of Thermogravimetric Data, *J. Appl. Polym. Sci.*, 1961, **5**, 285–292.

32 M. Fineman and S. D. Ross, Linear method for determining monomer reactivity ratios in copolymerization, *J. Polym. Sci.*, 1995, **5**, 259–262.

33 V. Jankus and A. P. Monkman, Is Poly(Vinylcarbazole) a Good Host for Blue Phosphorescent Dopants in PLEDs? Dimer Formation and Their Effects on the Triplet Energy Level of Poly(*N*-Vinylcarbazole) and Poly(*N*-Ethyl-2-Vinylcarbazole), *Adv. Funct. Mater.*, 2011, **21**, 3350–3356.

34 S. A. Bagnich, S. Athanasopoulos, A. Rudnick, P. Schroegel, I. Bauer, N. C. Greenham, P. Strohriegl and A. Kohler, Excimer Formation by Steric Twisting in Carbazole and Triphenylamine-Based Host Materials, *J. Phys. Chem. C*, 2015, **119**, 2380–2387.

35 A. Iraqi, T. G. Simmance, H. Yi, M. Stevenson and D. G. Lidzey, Preparation and Properties of 4-Dialkylaminophenyl *N*-Functionalized 2,7-Linked Carbazole, Polymers, *Chem. Mater.*, 2006, **180**, 5789–5797.

36 X. G. Li, M.-R. Huang, W. Feng, M.-F. Zhu and Y.-M. Chen, Facile synthesis of highly soluble copolymers and sub-micrometer particles from ethylaniline with anisidine and sulfoanisidine, *Polymer*, 2004, **45**, 101–115.

37 G. Inzlet, Formation and redox behaviour of polycarbazole prepared by electropolymerization of solid carbazole crystals immobilized on an electrode surface, *J. Solid State Electrochem.*, 2003, **7**, 503–510.

38 S. Tiptipakorn, S. D. Ando, K. Hemvichian and S. Rimdusit, Thermal degradation behaviors of polybenzoxazine and silicon-containing polyimide blends, *Polym. Degrad. Stab.*, 2007, **92**, 1265–1278.

39 T. Agag and T. Takeichi, Novel method for preparation of poly(benzoxazinone-imide), *Polym. Chem.*, 2000, **38**, 1647–1655.

